

## Article

# Application of Silicon Dioxide as the Inert Component or Oxide Component Enhancer in ANFO

Andrzej Biessikirski <sup>1,\*</sup>, Krzysztof Barański <sup>1</sup>, Mateusz Pytlik <sup>2</sup>, Łukasz Kuterasiński <sup>3</sup>,  
Jolanta Biegańska <sup>1,4</sup> and Konrad Słowiński <sup>1</sup>

<sup>1</sup> Faculty of Mining and Geoengineering, AGH University of Science and Technology, Al. Mickiewicza 30, 30-059 Kraków, Poland; baranski@agh.edu.pl (K.B.); biega@agh.edu.pl (J.B.); slwkonrad1997@gmail.com (K.S.)

<sup>2</sup> Conformity Assessment Body, Central Mining Institute, Plac Gwarków 1, 40-166 Katowice, Poland; mpytlik@gig.eu

<sup>3</sup> Jerzy Haber Institute of Catalysis and Surface Chemistry, Polish Academy of Sciences, ul. Niezapominajek 8, 30-239 Kraków, Poland; nckutera@cyf-kr.edu.pl

<sup>4</sup> Faculty of Energy and Fuels, AGH University of Science and Technology, Al. Mickiewicza 30, 30-059 Kraków, Poland

\* Correspondence: abiess@agh.edu.pl; Tel.: +48-12-67-20-70

**Abstract:** Non-ideal explosives with differing contents of silicon dioxide (silica or dioxosilane) added in the form of powder and gel were tested. Measurements of structure, crystallinity and morphology were performed by means of infrared spectroscopy (IR), X-ray diffraction (XRD) and scanning electron microscopy (SEM). IR and XRD analysis revealed a lack of SiO<sub>2</sub> influence on the non-ideal explosive structure. SEM analysis indicated that all the surface deformations of ammonium nitrate(V) prill were filled by a thin fuel film layer on which SiO<sub>2</sub> was present. The additional calculations of selected theoretical properties of non-ideal compositions were made using ZMWCyw software. Based on this, it was established that the optimum semimetal content was 1.0 wt.%. Blasting tests confirmed that the addition of 1.0 wt.% SiO<sub>2</sub> to the Ammonium Nitrate Fuel Oil (ANFO) resulted in the lowest volume of post-blast fumes. Moreover, it was established that finer SiO<sub>2</sub> powder cannot be used as the oxide component enhancer due to the inhibition of detonation reaction. SiO<sub>2</sub> should be used only as an inert component.

**Keywords:** ANFO; silicon dioxide; post-blast fumes; velocity of detonation



**Citation:** Biessikirski, A.; Barański, K.; Pytlik, M.; Kuterasiński, Ł.; Biegańska, J.; Słowiński, K. Application of Silicon Dioxide as the Inert Component or Oxide Component Enhancer in ANFO. *Energies* **2021**, *14*, 2152. <https://doi.org/10.3390/en14082152>

Received: 16 March 2021

Accepted: 8 April 2021

Published: 12 April 2021

**Publisher's Note:** MDPI stays neutral with regard to jurisdictional claims in published maps and institutional affiliations.



**Copyright:** © 2021 by the authors. Licensee MDPI, Basel, Switzerland. This article is an open access article distributed under the terms and conditions of the Creative Commons Attribution (CC BY) license (<https://creativecommons.org/licenses/by/4.0/>).

## 1. Introduction

Ammonium nitrate-based explosives are defined as mixtures of ammonium nitrate(V) with various types of fuel oils. They are currently the subject of wide interest due to their simplicity of manufacture and the wide range of possible blasting property modifications. However, since the measured velocity of detonation (VOD) does not reach its theoretically predicted values, and it does not show a non-ideal type of behaviour with the critical diameter, ammonium nitrate-based explosives should be included in the non-ideal type of explosives [1,2]. This can be explained by the length of the chemical reaction zone, which is much longer due to the slow secondary type of reactions [1,3,4].

According to the Zeldovich-Neumann-Doering theory of detonation, the energy value of non-ideal high explosives depends on their chemical composition and charge diameter. This means that it is possible to adjust detonation parameters due to the composition modification. However, obtained properties will differ from those calculated on the basis of thermodynamic estimates [5,6].

The addition of metal or inert components to the non-ideal explosive composition was made in order to obtain the desired blasting properties, to replace the fuel or oxide component or to improve oxygen balance. At present, the most commonly applied non-organic fuel component which can be used to replace fuel oil is aluminium. Maranda as

well as Kramarczyk et al. have studied the influence of various types of aluminium oxides on explosive properties [7,8]. Buczkowski examined the detonation properties of mixtures of milled ammonium nitrate(V)-based fertilizers and fuels, aluminium and mineral oil [9]. Moreover, it was reported that non-ideal explosive composition with a high content of aluminium would detonate [9]. Zygmunt confirmed that the most effective sensitizer of AN was aluminium [10]. Maranda showed that the VOD of a non-ideal explosive with aluminium content increases to a certain point (ca. up to 18–20%) with an increased content of metal [7]. Biessikirski et al. investigated the influence of the application possibility of copper, magnesium, aluminium and zinc powders of a similar grain size on the heat of the explosion. It was concluded that aluminium and magnesium powders gave the highest values of explosion heat, which could be explained by the high heat of the combustion of the tested metals [11]. Anderson et al. attempted to improve insensitive munition response, but also maintain the performance of aluminized formulations, by substituting aluminium with silicon [12]. They concluded that the obtained measurements of the heat released were close to the results of LX-14 (a mixture of a high melting explosive with Estane and 5702FI plastic binders) [12]. Barański tested the possible application of silicon and bismuth compositions in pyrotechnical elements. He indicated that the most promising delay in pyrotechnic compositions are those containing 40 wt.% of silicon due to them being of higher stability and the repeatability of their combustion process [13]. Furthermore, the application of an inert component influences either the blasting properties of explosives materials or the burning characteristics of pyrotechnic delay elements in detonators (e.g., the time of burning). The main reason for silica or bismuth oxide application in pyrotechnical elements is the shift towards green explosives.

The aim of this paper was to describe the possible influence of silicon dioxide powder on non-ideal explosive morphology, as well as on selected blasting and the physical properties of explosive materials. It should be noted that, according to Keshavarz et al. non-ideal explosives will not completely match the Chapman-Jouguet theory, because they do not reach the assumptions of instantaneous thermodynamic equilibrium. This may result in different values between detonation properties which are established through thermodynamic calculations and in situ tests. Those differences can be explained by the equilibrium model of one-dimensional and steady-state calculations [14]. The selection of SiO<sub>2</sub> can be explained by its high availability, favourable oxygen balance, high density and high boiling point.

## 2. Materials and Methods

### 2.1. Materials

Ammonium nitrate porous prill (AN-PP) was produced by Yara's International in 2020. The AN-PP density was ca. 820 kg·m<sup>-3</sup>, and the prill density did not exceed 1 mm. The moisture content was beneath 0.3 wt.%.

Three different samples of silicon dioxide (M1, M2, M3) were investigated. Silicon dioxide sample M1 and sample M2 were produced by Solvay. They were characterized by 98.0% purity and a density of 2200 kg·cm<sup>-3</sup> and 2100 kg·cm<sup>-3</sup>. The grain sizes of sample M1 and sample M2 were, respectively, 44 and 63 µm.

SiO<sub>2</sub> sample M3 was in the form of a grain gel. It was produced by GIEBEL FilTec GmbH. The grain size was in the range of 1.5–2.0 mm and the density was 750 kg·cm<sup>-3</sup>.

The fuel oil (FO) was a wide-range sample which was produced in 2020. The sample density and kinetic viscosity at 40 °C were 800 kg·m<sup>-3</sup> and 13.6 mm<sup>2</sup>·s<sup>-1</sup>, respectively. The physio-chemical properties of the FO are described in [15].

All ANFO samples were prepared by blending AN-PP with FO for 25 min at 250 rpm, using a mixer. Silicon dioxide was added to the ANFO for the last 10 min of the blending process. General sample compositions are presented in Table 1.

**Table 1.** General chemical composition of non-ideal explosives, % by mass (without the distinction between M1, M2 and M3 silica type).

Non-Ideal Explosive	Content, wt.%		
	AN-PP	FO	SiO <sub>2</sub>
Sample 1	94.0	6.0	-
Sample 2	94.0	5.0	1.0
Sample 3	94.0	4.0	2.0
Sample 4	93.07	5.94	0.99
Sample 5	92.15	5.89	1.96

## 2.2. Instrumental Methods

The FT-IR measurements were performed using a iS-10 spectrometer from Thermo Scientific (Madison, WI, USA), equipped with an MCT detector and ATR adapter. The IR spectra range was 650–4000 cm<sup>-1</sup> with 32 scans per spectrum.

The X-ray powder diffraction (XRD) experiments were conducted with a PANalytical X'Pert PRO MPD diffractometer with CuK $\alpha$  radiation at 40 kV and 30 mA (Malvern PANalytical Ltd., Malvern, UK). The scanning was performed at 5–50° 2 $\theta$  range with a 0.033° step at room temperature. The studied ANFO samples were in powder form and were placed in holders.

The scanning of electron micrographs of ANFO samples was carried out using Nova NanoSEM 200 from FEI Europe (5–18 keV) (Hillsboro, OR, USA). Scans were taken in a low vacuum ca. 60 Pa with a low vacuum detector (LVC), operating in secondary electron mode under magnifications of 50–1000 $\times$ . The samples were placed in the holders, using double-sided, conductive, vacuum compatible carbon tape. Before the analysis, the samples were covered with a carbon layer. The electron beam voltage was 10 kV. Before coating, the explosive matrix samples were dried (under standard conditions) for 24 h.

## 2.3. Thermodynamic Models

Thermodynamic calculations were made using the ZMWCyw software which was developed by the Military University of Technology in Warsaw. Oxygen balance was calculated based on the standard [16]. The ZMWCyw software enabled the calculation of standard energy, explosion pressure, explosion temperature, the heat of the explosion, the post-blast volume based on the non-ideal explosive composition and the physicochemical properties of each individual component.

## 2.4. Blasting Tests

The velocity of detonation (VOD) was determined using the start-stop method [17]. The ANFO charge was placed in a glass tube of 46.4 mm inner diameter. Two short circuit probes were placed throughout the charge. The distance between the probes was 150 mm. The distance between the primer and start signal probe was equal to two charge diameters. The measurement consisted of the time difference that described the first recorded signal change in each probe. VOD was calculated according to Equation (1):

$$\text{VOD} = \frac{l}{t} \quad (1)$$

where  $l$  is the test base distance between the two probes and  $t$  is the time difference.

The 14 g RDX-based (Royal Demolition Explosive) charge primed the detonation.

Post-blast oxides were measured according to the standard [18], which is complied with the European directive [19]. Non-ideal explosive samples of a mass of 600 g were detonated in the blasting chamber. After the detonation, post-blast fumes were homogenized for a 3 min, using fan system. After homogenization, post-blast gases were collected for 20 min in the ventilation system. The amounts of CO<sub>x</sub> and NO<sub>x</sub> were determined by IR (MIR 25e) and chemiluminescent (TOPAZE 32M) analyzers, respectively.

Both in the case of VOD and post-blast research, five individual shoots were made.

### 3. Results and Discussion

#### 3.1. Morphology of Non-Ideal Explosives with the Addition of Silicon Dioxide

For all samples (Figure 1), the bands at 3230–2852  $\text{cm}^{-1}$  could be attributed to an asymmetric ammonium cation stretching mode and to asymmetric ammonium cation vibration deformation. The band at 1753  $\text{cm}^{-1}$  could be assigned to an  $\text{NO}_3^-$  in-plane deformation and stretching vibration or could correspond to a combination of an asymmetric ammonium cation deformation with a lattice mode. The occurrence of intensive maxima at 1410 and 1290  $\text{cm}^{-1}$  probably originated from the triply degenerated deformation of  $\text{NH}_4^+$  and the doubly degenerated stretching vibration of nitrate anion. The bands at 1041 and 825  $\text{cm}^{-1}$  indicate symmetrical  $\text{NO}_3^-$  in-plane stretching and  $\text{NO}_3^-$  out-of-plane deformation [15,20–23]. The bands at 2921 and 2852  $\text{cm}^{-1}$  implied  $-\text{CH}_2-$  and  $-\text{CH}_3$  stretching vibrations which were coming from the FO [24]. The rest of the bands assigned to FO overlapped with the bands of AN skeletal vibrations. The bands attributed to powder or gel  $\text{SiO}_2$  (both with 1 wt.% and 2 wt.% addition) were not found.

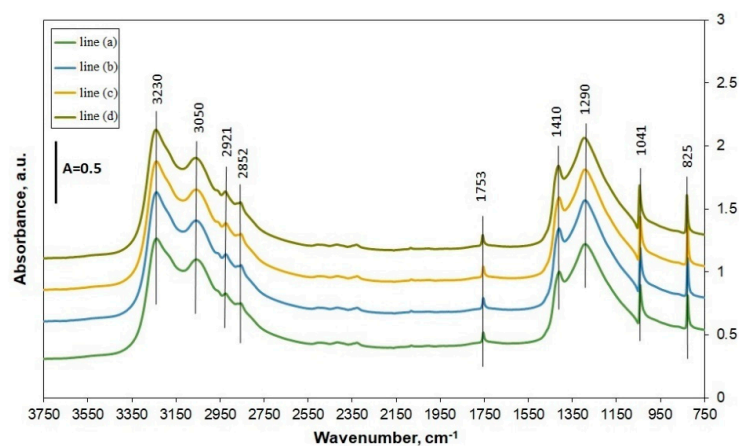


**Figure 1.** IR spectra of non-ideal explosives: (a) sample 1; (b) sample 3 with M1; (c) sample 3 with M2; (d) sample 3 with M3.

The analysis of XRD images indicated the presence of ammonium nitrate with a  $P_{mnm}$  space group and two molecules per unit cell [25–27], Figure 2. The addition of FO and silica to AN-PP caused the appearance of reflexes at  $28^\circ$  and  $47^\circ$ , which originated from the (111) and (220) silica phase [28]. Due to the amorphous phase of M3, this sample was not subjected to XRD research.

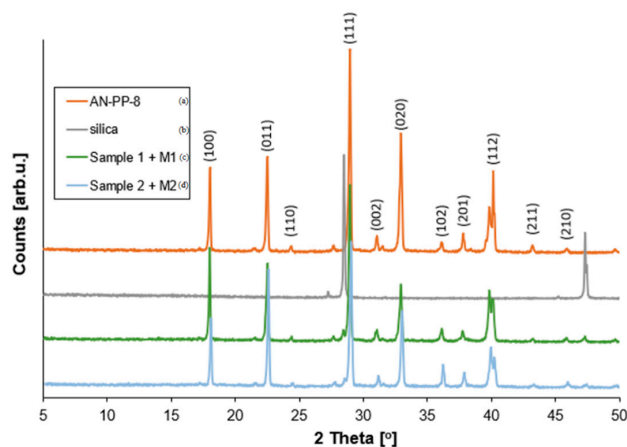


**Figure 2.** XRD patterns of: (a) AN-PP, (b) silicon dioxide, and non-ideal explosives: (c) Sample 1 + M1, (d) Sample 2 + M2.

A typical crystal of ammonium nitrate(V) porous prill was characterized by the presence of wrinkles both on the prill surface, as well as in the cross-section of the prill. The addition of FO to the AN caused all surface deformations, cracks and pores to be filled. [2,26,27,29–33]. The addition of silicon dioxide to the ANFO did not change the morphology of the sample, as shown in Figure 3a–d.

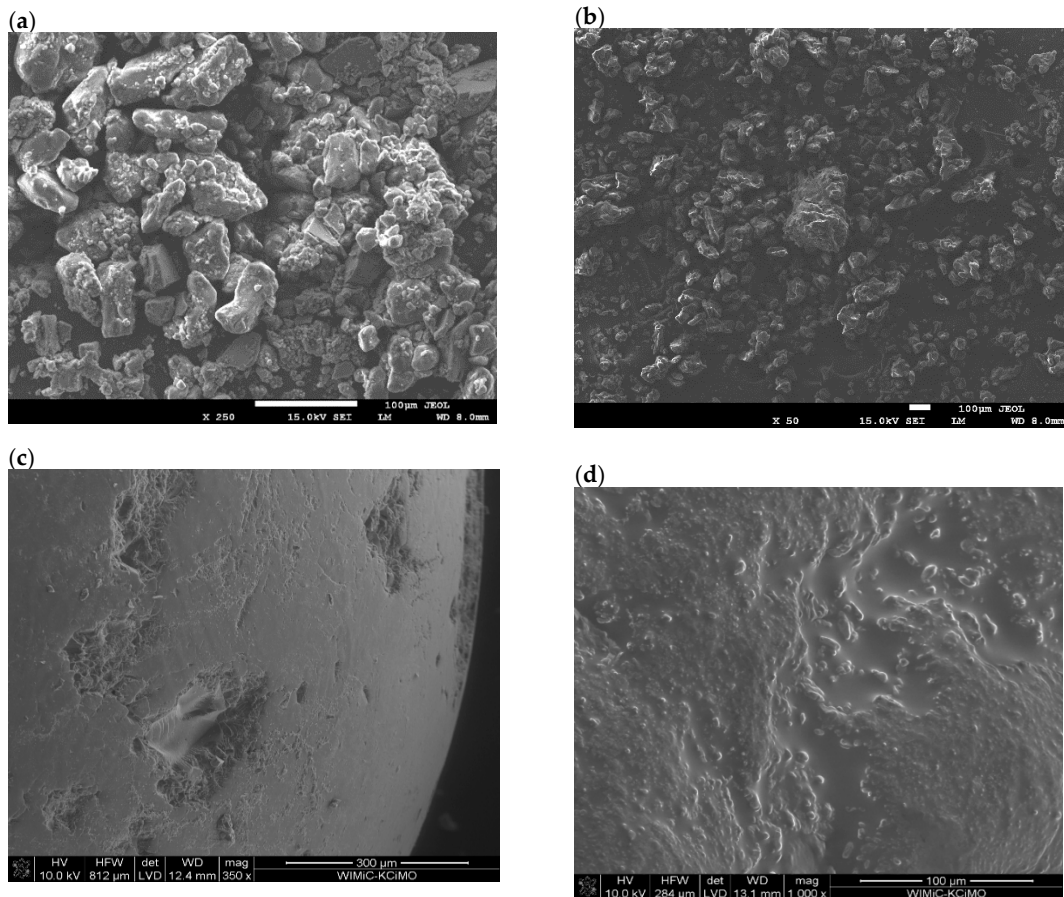


**Figure 3.** Results of SEM: (a) sample 1—magnification of 250×; (b) sample 2—magnification of 50×; (c) sample 3—magnification of 350×; (d) sample 3—magnification of 1000×.

Based on Figure 3a, it can be concluded that the silicon dioxide from a grain size of 44  $\mu\text{m}$  covered a thin fuel film layer, which was present on the surface of the AN. The increased content of the semimetal (Figure 3a) caused full coverage of AN prill by an inert semimetal, which in the case of silica could inhibit the detonation reaction. In the case of silicon dioxide from the grain size of 63  $\mu\text{m}$ , Figure 3b, the silica grains covered the fuel film layer, as they did in the case of the silica grain size of 44  $\mu\text{m}$ ; however, some free gaps and voids between grains were visible. This effect can have an influence on the diffusion-controlled reactions. In both cases,  $\text{SiO}_2$ , which was present in the fuel film layer, filled all the voids and surface deformations which were present on the surface of the prill. In the case of the gel silicon dioxide, displayed in Figure 3c, the surface of the granule was rather flat with a low number of surface deformations. The thin fuel film layer was present on the granule surface; however, with time, a dribbling effect can appear. The surface of the granule is similar to the typical fertilizer grade ammonium nitrate granule. In the case of a non-ideal explosive with M3 addition, the fuel film layer was present both on the crystal surface of AN-PP (Figure 3d) and silica. This should be explained by the size differentiation between AN-PP granule and M3 powder. However, due to the size differentiation between the AN-PP granule and the M3 powder, silica did not cover the thin film fuel layer which was present on the surface of the AN-PP granule. This was

contrary to the non-ideal explosive samples with the addition of M1 and M2. Based on the SEM analysis, it can be concluded that the addition of silicon dioxide should not influence the non-ideal morphology. However, by taking into consideration silica combustibility, it can be assumed that the detonation reaction may be inhibited, especially in the case of the silicon dioxide of 44  $\mu\text{m}$  grain size.

### 3.2. Morphology of Non-Ideal Explosives with Silicon Dioxide Addition

Evaluated non-ideal parameters in ZMWCyw software are presented in Tables 2 and 3.

**Table 2.** Simulated properties of non-ideal explosives with silicon dioxide powder as an oxide component enhancer.

Parameter	Composition: AN-PP:FO:SiO <sub>2</sub>				
	94.0:6.0:0.0	94.0:5.5:0.5	94.0:5.0:1.0	94.0:4.5:1.5	94.0:4.0:2.0
Energy, $\text{kJ}\cdot\text{kg}^{-1}$	−4274	−4340	−4406	−4472	−4538
Detonation pressure, MPa	2797	2822	2770	2701	2628
Detonation temperature, K	2663	2693	2613	2513	2411
Heat of explosion, $\text{kJ}\cdot\text{kg}^{-1}$	3958	3994	3809	3588	3367
Strength of explosion, $\text{kJ}\cdot\text{kg}^{-1}$	973	969	934	894	854
Post-blast volume, $\text{L}\cdot\text{kg}^{-1}$	997	982	976	971	967
Density, $\text{kg}\cdot\text{m}^{-3}$	830	839	848	857	866
Oxygen balance, %	−2.10	−0.354	1.39	3,13	4.87

**Table 3.** Simulated properties of non-ideal explosive as an inert component.

Parameter	Composition: AN-PP:FO:SiO <sub>2</sub>		
	93.53:5.97:0.5	92.15:5.89:1.96	93.07:5.94:0.99
Energy, $\text{kJ}\cdot\text{kg}^{-1}$	−4274	−4382	−4485
Detonation pressure, MPa	2797	2828	2898
Detonation temperature, K	2663	2646	2627
Heat of explosion, $\text{kJ}\cdot\text{kg}^{-1}$	3958	3920	3881
Strength of explosion, $\text{kJ}\cdot\text{kg}^{-1}$	973	956	941
Post-blast volume, $\text{L}\cdot\text{kg}^{-1}$	997	987	978
Density, $\text{kg}\cdot\text{m}^{-3}$	830	839	857
Oxygen balance, %	−2.10	−2.07	−2.04

The addition of SiO<sub>2</sub> to the ANFO composition was researched in two different case studies, independently of the grain diameter. Table 2 shows the influence of SiO<sub>2</sub> as an oxide component enhancer on ANFO blasting properties. Table 3 indicates the influence of SiO<sub>2</sub> as a general inert component on ANFO blasting properties. In general, when the semimetal component has been added to the non-ideal composition, an inert component combusts behind the reaction front zone. As a result, the detonation temperature and pressure increased, which could be explained by the growth of the surface, which is responsible for the heat exchange between the semimetal grains and the individual product of the explosives' decomposition reaction, as well as by the improved zone of the chemical reaction [7]. However, dioxosilane, as a typical non-combustion compound, is generally chemically unreactive. This means that SiO<sub>2</sub> can be treated as an inert component, which mainly influences the density of the non-ideal composition, as well as oxygen balance. Density changes, as well as the differentiation of the oxygen balance, is followed based on the conservation of mass and momentum equations (relationships between detonation pressure, velocity and post-blast volume) by the change of the detonation reaction conditions, which causes a shift in the Chapman-Jouguet plane and finally influences blasting properties. With a change in the oxygen balance, the heat of the explosion should also change. It has been established that explosives with the 0 oxygen balance have the highest heat of the explosion. Based on Table 2, it can be observed that, in theory, the non-ideal composition of AN-PP:FO:SiO<sub>2</sub> has the oxygen balance which is closest to 0 which results in the highest heat of the explosion of ca. 3994  $\text{kJ}\cdot\text{kg}$ . A further increase in positive and

negative oxygen balance was followed by a decrease in the heat of the explosion, which from Hugoniot's equation is connected with a decrease in detonation temperature and pressure, Table 2.

The results of the post-blast volume indicate that SiO<sub>2</sub> is a non-combustion compound and that a drop in the post-blast volume will be caused by a decreased content of fuel oil. However, it is expected that with a more positive oxygen balance, the content of the NO<sub>x</sub> in post-blast fumes will increase. Moreover, the addition of the SiO<sub>2</sub> results in increasing influence on the density of non-ideal explosive, which by taking the known reaction density–VOD should result in an improved VOD. Similar results were obtained when the SiO<sub>2</sub> was treated as a typical inert component, as can be seen in Table 4. In this scenario, the ratio between AN-PP and FO is maintained, which mainly leads to the influence of the oxygen which is present in the SiO<sub>2</sub> on the explosive's oxygen balance. However, due to the fact that the content of FO should not change, improvement of the oxygen balance is much slower. In the case of the 2.0% silica addition as the inert component, the oxygen balance was of ca. −2.0%; and in the case of 2.0% silica addition, when SiO<sub>2</sub> was influencing the oxide component, the oxygen balance was ca. of 5.0 wt.%, as shown in Table 2. An increase in the temperature and detonation pressure should be present until the oxygen balance of the non-ideal explosive reaches 0. This will also be followed with the lower content of toxic fumes in the post-blast oxides.

**Table 4.** Average results of velocity of detonation (VOD) and post-blast fumes of non-ideal explosive with SiO<sub>2</sub> addition as an oxide component enhancer.

Parameter	Type and Size of SiO <sub>2</sub>	Composition: AN-PP:FO:SiO <sub>2</sub>		
		94.0:6.0:0.0	94.0:5.0:1.0	94.0:4.0:2.0
Density, kg·m <sup>−1</sup>		801	673	703
VOD, m·s <sup>−1</sup>		1622	485	N/D
Volume of CO <sub>2</sub> , dm <sup>3</sup> ·kg <sup>−1</sup>	Powder, 44 μm (M1)	94.19	83.66	N/D
Volume of CO, dm <sup>3</sup> ·kg <sup>−1</sup>		13.91	4.70	N/D
Volume of NO, dm <sup>3</sup> ·kg <sup>−1</sup>		1.53	7.57	N/D
Volume of NO <sub>2</sub> , dm <sup>3</sup> ·kg <sup>−1</sup>		0.11	0.54	N/D
Volume of NO <sub>x</sub> , dm <sup>3</sup> ·kg <sup>−1</sup>		1.64	8.11	N/D
Density, kg·m <sup>−1</sup>		801	753	770
VOD, m·s <sup>−1</sup>		1622	1609	1659
Volume of CO <sub>2</sub> , dm <sup>3</sup> ·kg <sup>−1</sup>	Powder, 63 μm (M2)	94.19	106.02	107.53
Volume of CO, dm <sup>3</sup> ·kg <sup>−1</sup>		13.91	5.87	5.94
Volume of NO, dm <sup>3</sup> ·kg <sup>−1</sup>		1.53	12.92	12.81
Volume of NO <sub>2</sub> , dm <sup>3</sup> ·kg <sup>−1</sup>		0.11	2.71	2.78
Volume of NO <sub>x</sub> , dm <sup>3</sup> ·kg <sup>−1</sup>		1.64	15.63	15.59
Density, kg·m <sup>−1</sup>		801	794	844
VOD, m·s <sup>−1</sup>		1622	422	N/D
Volume of CO <sub>2</sub> , dm <sup>3</sup> ·kg <sup>−1</sup>	Granule, 1.5–2.0 mm (M3)	94.19	120.04	N/D
Volume of CO, dm <sup>3</sup> ·kg <sup>−1</sup>		13.91	4.47	N/D
Volume of NO, dm <sup>3</sup> ·kg <sup>−1</sup>		1.53	12.43	N/D
Volume of NO <sub>2</sub> , dm <sup>3</sup> ·kg <sup>−1</sup>		0.11	1.89	N/D
Volume of NO <sub>x</sub> , dm <sup>3</sup> ·kg <sup>−1</sup>		1.64	14.33	N/D

Moreover, according to Anderson et al., high detonation temperature and pressure result in the rapid melting and atomization of the silicon, which subsequently reacts with oxygen-bearing detonation gases. Furthermore, Anderson et al. stated that it is possible that not all of the silicon will react by expanding. This could be explained by a rapid decrease in the temperature, which upon an adiabatic expansion of gases, is further followed by insufficient temperatures and heat flux to fully atomize all silicon [12,34].

### 3.3. Results of Blasting Tests

Results of blasting properties of non-ideal explosives with silicon addition are presented in Tables 4 and 5.

**Table 5.** Average results of VOD and post-blast fumes of non-ideal explosive with SiO<sub>2</sub> addition as an inert component.

Parameter	Type and Size of SiO <sub>2</sub>	Composition: AN-PP:FO:SiO <sub>2</sub>		
		94.0:6.0:0.0	92.15:5.89:1.96	93.07:5.94:0.99
Density, kg·m <sup>-1</sup>		733	667	699
VOD, m·s <sup>-1</sup>		2230	1609	2568
Volume of CO <sub>2</sub> , dm <sup>3</sup> ·kg <sup>-1</sup>	Powder, 44 μm (M1)	92.63	90.37	92.81
Volume of CO, dm <sup>3</sup> ·kg <sup>-1</sup>		5.70	5.09	6.28
Volume of NO, dm <sup>3</sup> ·kg <sup>-1</sup>		1.53	2.18	10.57
Volume of NO <sub>2</sub> , dm <sup>3</sup> ·kg <sup>-1</sup>		0.18	0.22	1.44
Volume of NO <sub>x</sub> , dm <sup>3</sup> ·kg <sup>-1</sup>		1.71	2.41	12.01
Density, kg·m <sup>-1</sup>		733	715	721
VOD, m·s <sup>-1</sup>		2230	2451	2509
Volume of CO <sub>2</sub> , dm <sup>3</sup> ·kg <sup>-1</sup>	Powder, 63 μm (M2)	92.63	92.77	93.06
Volume of CO, dm <sup>3</sup> ·kg <sup>-1</sup>		5.70	2.75	4.88
Volume of NO, dm <sup>3</sup> ·kg <sup>-1</sup>		1.53	8.08	9.63
Volume of NO <sub>2</sub> , dm <sup>3</sup> ·kg <sup>-1</sup>		0.18	1.26	1.64
Volume of NO <sub>x</sub> , dm <sup>3</sup> ·kg <sup>-1</sup>		1.71	9.34	11.27
Density, kg·m <sup>-1</sup>		733	732	747
VOD, m·s <sup>-1</sup>		2230	2093	2196
Volume of CO <sub>2</sub> , dm <sup>3</sup> ·kg <sup>-1</sup>	Granule, 1.5–2.0 mm (M3)	92.63	91.58	92.35
Volume of CO, dm <sup>3</sup> ·kg <sup>-1</sup>		5.70	4.89	5.12
Volume of NO, dm <sup>3</sup> ·kg <sup>-1</sup>		1.53	3.04	3.83
Volume of NO <sub>2</sub> , dm <sup>3</sup> ·kg <sup>-1</sup>		0.18	0.46	0.66
Volume of NO <sub>x</sub> , dm <sup>3</sup> ·kg <sup>-1</sup>		1.71	3.50	4.48

The obtained results of SiO<sub>2</sub> addition with ANFO as the oxidizer enhancer show the limitations of this approach, as displayed in Table 4. In the case of the SiO<sub>2</sub> of 44 μm (M1) and silica gel (M3), a lack of detonation (N/D) was observed regardless of the silica content (1.0 wt.%, or 2.0 wt.%). With an increase in the powder SiO<sub>2</sub> grain size (application of M2), the detonation process did occur, as shown in Table 4. These differences can be explained by the mechanism of the detonation reaction. In the case of the heterogeneous explosives (ANFO), the detonation process relies upon the intermolecular reactions which are influenced by, for example, the voids or air. In other words, intermolecular reactions are diffusion-controlled processes which are affected by all internal and external factors. These factors have an effect on the rate of the transport of the reactant which ultimately inhibits or stimulates the detonation process. Based on the SEM analysis, it can be seen that finer silica grains (M1) have fully covered the whole fuel film layer, which resulted in no voids. Moreover, by taking into consideration the fact that SiO<sub>2</sub> is a typical non-combustion compound, it can be concluded that it also inhibits the progression of the detonation process. In the case of the silica gel, existing voids and the limited surface of contact between fuel and the oxygen component was probably responsible for the heat lost, which has also resulted in no detonation process.

The application of silica as an oxide component enhancer primarily affects the oxygen balance of the non-ideal explosive composition and secondly, the physical parameters of the non-ideal explosives. This can be observed especially in the case of NO<sub>x</sub> and CO<sub>2</sub> volume in post-blast fumes. The application of silica as the oxide component enhancer resulted in a shift of the oxygen balance towards positive values. This can be explained by the lowering of FO content, as well as the additional introduction of oxygen which is present in the silica compound. The shift towards positive oxygen balance resulted, in both cases, in a high increase in the NO<sub>x</sub> and CO<sub>2</sub> volume. An increase in the CO<sub>2</sub> can be explained by the complete oxidation of the CO (which is formed as a step-product) by the additionally

available oxygen (e.g., pure ANFO  $94.19 \text{ dm}^3 \cdot \text{kg}^{-1}$ , non-ideal explosive with 1.0 wt.% of M2  $106.02 \text{ dm}^3 \cdot \text{kg}^{-1}$  and non-ideal explosive with 2.0 wt.% of M2  $107.53 \text{ dm}^3 \cdot \text{kg}^{-1}$ ). Furthermore, as previously mentioned, the application of  $\text{SiO}_2$  resulted in the influence on the density of the non-ideal explosives. Based on the strata obtained, it can be observed that VOD rose with as the density of the non-ideal composition increased. This observation is in accordance with the typical density–VOD relation, as well as with the conclusion derived from the theoretical calculation. A detailed analysis of the influence of dioxosilane on the physical and blasting properties of the non-ideal explosive will be discussed in more detail.

It should be noted that silica addition to the explosive composition, due to its non-combustible properties, resulted in the improved sensitivity of the explosive material. This means that this type of explosive should require greater critical diameter and priming energy in order to initiate and sustain the detonation reaction. It should also be considered that the shock wave which progressed through the non-ideal explosive charge compressed the explosive layers which were ahead of the wave front, which resulted in an influence on the temperature and the chemical reaction. In order to excite and stimulate the detonation, a high velocity should be obtained, however, finer silica grains and silica gel granule probably do not allow this, as shown in Table 4. In other words, the velocity was probably not at a sufficient level to increase the temperature due to compression. This was especially visible in the case of the non-ideal explosive samples with 1.0% wt. M1 and M2, where the obtained post-blast volume of fumes, as well as the velocity of the decomposition reaction ( $<1000 \text{ m} \cdot \text{s}^{-1}$ ) indicated that the tested samples had undergone an explosion reaction instead of detonation. A further increase in the silica in the composition would lead to a misfire. A similar situation (possible explosion or the presence of misfires) is expected in the case where dioxosilane would be used as a fuel enhancer. In these cases, the silica addition would result in a lower content of AN-PP. This should not have as much of an effect on the oxygen balance of the composition due to the additional presence of oxygen in silica, however, the lower content of AN-PP would result in a smaller content of  $-\text{NO}_2$  which is responsible for the detonation reaction. Furthermore, this would also lead to an increase in the critical diameter, as well as to a decrease in the sensitivity, like in the case of the oxide component enhancer approach. On the other hand, this would probably result in a high amount of misfires due to the lower content of the nitrous group.

The results of the blasting parameters present the possible application of dioxosilane as a typical inert component, as shown in Table 5.

The application of  $\text{SiO}_2$  as a typical inert material resulted in a detonation process in all of the investigated cases, as shown in Table 5. It was observed that VOD increased with the silica content. This can be explained by the influence of the inert component on the non-ideal explosive density. However, it should be noted that in the case of silica powder with a grain size of  $44 \mu\text{m}$ , the VOD of the non-ideal explosive with 1.0 wt.% silicon dioxide addition was lower ( $1609 \text{ m} \cdot \text{s}^{-1}$ ) in comparison with the VOD of pure ANFO ( $2240 \text{ m} \cdot \text{s}^{-1}$ ). In the case of the 1.0 wt.% addition of the silica powder, which was characterised by a grain size of  $63 \mu\text{m}$ , the non-ideal explosive VOD was higher ( $2451 \text{ m} \cdot \text{s}^{-1}$ ) than the pure ANFO ( $2240 \text{ m} \cdot \text{s}^{-1}$ ). The VOD of 1.0 wt.% addition of the silica gel case ( $2093 \text{ m} \cdot \text{s}^{-1}$ ) is close to the VOD of pure ANFO. These results were contrary to the results obtained for the non-ideal explosive with the  $44 \mu\text{m}$  silica addition. An increase in the VOD with the silica content could also be explained by the differences between densities. The lower VOD for the non-ideal explosive sample (with 1.0 wt.% addition of M1) in comparison with pure ANFO, could be explained by the significant differences between densities, respectively, from  $667 \text{ kg} \cdot \text{m}^{-3}$  to  $733 \text{ kg} \cdot \text{m}^{-3}$ . An increase in the charge density resulted in a reduction in the distance between prills. Smaller distances have a direct impact on the hot spots' appearance (smaller gaps between neighbouring hot spots) which in the end causes lower heat loss [34]. In the case of the explosive sample, where only the content of the inert components influences the general density of the composition, higher charge density improves the chemical reaction zone which usually influences the heat exchange and reduction in the heat loss. The effect of this is that the detonation temperature rises,

which further results in the higher heat of the explosion and VOD. It can be assumed that the application of silica in correlation to the oxygen balance of the non-ideal explosives' composition can improve the heat of the explosion and VOD to a certain extent, as shown in Tables 3 and 5. Further increase in the silica can result in lower VOD values and in the possible presence of misfires due to the dead-pressed point.

In the case of the differences between grain diameters (Table 5), the voids which were established after dioxosilane addition caused the stimulation of the detonation process and higher VOD values. This can be explained by the diffusion and extended surface of the chemical reaction. However, in the case of the M3, the granule diameter is too big in comparison with M2, which directly leads to smaller surface contact and finally results in lower VOD (e.g., the VOD of non-ideal explosive samples with a 1.0 wt.% of M2 and M3 were, respectively,  $2451 \text{ m}\cdot\text{s}^{-1}$  and  $2093 \text{ m}\cdot\text{s}^{-1}$ ), as shown in Table 5. Moreover, with the increase in the inert component, the volume of the post-blast fumes changed. With this approach (when silica was added as an inert component), the general oxygen balance does not change as much as in the oxidizer enhancer approach. It resulted in similar changes (an increased volume of  $\text{CO}_2$  and  $\text{NO}_x$ , e.g.,  $\text{CO}_2$  and  $\text{NO}_x$  volume in the non-ideal explosive with 1.0 and 2.0 wt.% M3 content increased, respectively, from  $91.58 \text{ m}\cdot\text{s}^{-1}$  to  $92.35 \text{ m}\cdot\text{s}^{-1}$  and from  $3.50 \text{ m}\cdot\text{s}^{-1}$  to  $4.48 \text{ m}\cdot\text{s}^{-1}$ ), which can be explained by the slow shift of negative oxygen balance towards zero oxygen balance (Table 5).

#### 4. Conclusions

In this paper, the potential influence of silicon dioxide addition on a non-explosive structure and properties was presented.

Results obtained from XRD, IR and SEM analyses indicated zero influence from inert material on the non-ideal explosive structure and morphology.

Simulation of blasting properties indicated similar behaviour between both silica addition as a fuel component enhancer or inert materials. In both cases, it was shown that the highest values of detonation temperature, detonation pressure, heat of the explosion and post-blast fumes were obtained with 1.0 wt.% content of the inert component. The drop of all properties followed the further increase in semimetal. This could be explained by the increased zone of the reaction, as well as the elevated surface of heat exchange between grains of inert materials and individual products of the explosive decomposition reaction.

Blasting tests revealed that silica should be added only as an inert component. When silica is added as an oxidant component enhancer, the lack of the detonation was visible in the case of finer grains' powder and silica gel. Moreover, when silica was added as an inert component, an increase in the VOD was observed with the growth of the grain size. Despite this, the VODs of the explosive samples were greater in the case of the 2.0 wt.% inert component addition, and the optimum content of dioxosilane was 1.0 wt.% due to the lower concentration of post-blast fumes.

**Author Contributions:** Conceptualization, A.B.; methodology, A.B.; validation, A.B. and M.P.; formal analysis, A.B., M.P. and Ł.K.; investigation, A.B., M.P., Ł.K., K.B. and K.S.; resources, A.B., Ł.K. and M.P.; writing—original draft preparation, A.B., M.P., Ł.K., K.B., K.S. and J.B.; writing—review and editing, A.B.; visualization, A.B. and M.P.; supervision, A.B. All authors have read and agreed to the published version of the manuscript.

**Funding:** The authors wish to thank The Faculty of Mining and Geoengineering at the AGH University of Science and Technology in Krakow for their financial support for research no. 16.16.100.215.

**Institutional Review Board Statement:** Not applicable.

**Informed Consent Statement:** Not applicable.

**Data Availability Statement:** The data presented in this study are available on request from the corresponding author (A.B.).

**Conflicts of Interest:** The authors wish to confirm that there are no known conflict of interest associated with this publication and there has been no significant financial support for this work that could have influenced its outcome.

## References

1. Cummock, N.R.; Mares, J.O., Jr.; Gunduz, I.E.; Son, S.F. Relating a small-scale shock sensitivity experiment to large-scale failure diameter in an aluminized ammonium nitrate non-ideal explosive. *Combust. Flame* **2018**, *194*, 271–277. [[CrossRef](#)]
2. Miyake, A.; Takahara, K.; Ogawa, T.; Ogata, Y.; Wada, Y.; Arai, H. Influence of physical properties of ammonium nitrate on the detonation behavior of ANFO. *J. Loss Prev. Process. Ind.* **2001**, *14*, 533–538. [[CrossRef](#)]
3. Keshavarz, M.H.; Mofrad, R.T.; Poor, K.E.; Shokrollahi, A.; Zali, A.; Yousefi, M.H. Determination of performance of non-ideal aluminized explosives. *J. Hazard. Mater.* **2006**, *137*, 83–87. [[CrossRef](#)]
4. Davis, W.; Fauquignon, C. Classical theory of detonation. *J. Phys. IV Colloq.* **1995**, *5*, C4-3–C4-21. [[CrossRef](#)]
5. Smirnov, E.B.; Kostitsin, O.; Koval, A.V.; Akhlyustin, I.A. Model of non-ideal detonation of condensed high explosives. In Proceedings of the XXXI International Conference on Equations of State for Matter (ELBRUS 2016), Elbrus, Russia, 1–6 March 2016.
6. Paszula, J.M.; Kowalewski, E. Study of the detonation development of non-ideal explosives. *High-Energy Mater.* **2015**, *7*, 95–105.
7. Maranda, A. Influence of aluminum chemical activity on detonation parameters of composite explosive containing aluminum powders (CX-Al). *Wiad. Chem.* **2001**, *55*, 353–375.
8. Kramarczyk, B.; Pytlik, M.; Mertuszka, P. Effect of aluminium additives on selected detonation parameters of a bulk emulsion explosive. *High-Energy Mater.* **2020**, *12*, 99–113.
9. Buczkowski, D. Detonation properties of ammonium nitrate based fertilizers and fuels. *Cent. Eur. J. Energ. Mater.* **2011**, *8*, 99–106.
10. Zymunt, B. Detonation parameters of mixtures containing ammonium nitrate and aluminium. *Cent. Eur. J. Energ. Mater.* **2009**, *6*, 57–66.
11. Biessikirski, A.; Ziabka, M.; Dworzak, M.; Kuterasiński, Ł.; Twardosz, M. Effect of metal addition on ANFO's morphology and energy detonation. *Przem. Chem.* **2019**, *98*, 928–931.
12. Anderson, P.E.; Cook, P.; Kyle, A.D.; Mychajlonka, K.; Mileham, M. Silicon Fuel in High Performance Explosives. *Prop. Explos., Pyrotech.* **2014**, *39*, 74–78. [[CrossRef](#)]
13. Barański, K. Analysis of the Possibility of Using “Green Pyrotechnics” in the Detonators MW. Ph.D. Thesis, Faculty of Mining and Geoengineering, AGH University of Science and Technology in Cracow, Cracow, Poland, 27 September 2019.
14. Keshavarz, M.H.; Zamani, A.; Shafiee, M. Predicting detonation performance of CHNOFCl and aluminized explosives. *Prop. Explos. Pyrotech.* **2014**, *39*, 749–754. [[CrossRef](#)]
15. Biessikirski, A.; Wądrzyk, M.; Janus, R.; Biegańska, J.; Jodłowski, G.; Kuterasiński, Ł. Study on fuel oils used in ammonium nitrate-based explosives. *Przem. Chem.* **2018**, *97*, 457–462.
16. Niksiński, A. *Górnictwo Materiały Wybuchowe. Obliczanie Parametrów Użytkowych*; BN-80/6091-42; Zakłady Tworzyw Sztucznych ERG: Bierań, Poland, 1981.
17. Mertuszka, P.; Pytlik, M. Analysis and comparison of the continuous detonation velocity measurement method with the standard method. *High-Energy Mater.* **2019**, *11*, 63–72.
18. European Commission. *Explosives for Civil Uses. High Explosives. Part 16: Detection and Measurement of Toxic Gases*; EN 13631-16:2004; European Committee for Standardization: Brussels, Belgium, 2004.
19. European Union. Council directive 93/15/EEC of 5 April 1993 on the harmonization of the provisions relating to the placing on the market and supervision of explosives for civil uses. *Off. J. Eur. Union* **1993**, *12*, 20–36.
20. Sasoh, A.; Ogawa, T.; Takayama, K. Use of ammonium nitrate-alcohol (ANA) for ballistic range propellant. *J. Shock Waves.* **1999**, *9*, 291–294. [[CrossRef](#)]
21. Theoret, A.; Sandorfy, C. Infrared spectra and crystalline phase transitions of ammonium nitrate. *Can. J. Chem.* **1964**, *42*, 57–62. [[CrossRef](#)]
22. Biessikirski, A.; Kuterasiński, Ł.; Pyra, J.; Dworzak, M. Comparison of properties of ammonium nitrates used for production of fertilizers and explosive materials. *Przem. Chem.* **2016**, *95*, 1381–1384.
23. Wu, H.B.; Chan, M.N.; Chan, K. FTIR characterization of polymorphic transformation of ammonium nitrate. *Aerosol Sci. Technol.* **2007**, *41*, 581–588. [[CrossRef](#)]
24. Pretsch, E.; Bühlmann, P.; Badertscher, M. *Structure Determination of Organic Compounds. Tables of Spectral Data*; Springer: Berlin, Germany, 2009.
25. Hendricks, S.B.; Posnjak, E.; Kracek, F.C. Molecular rotation in the solid state. The variation of the crystal structure of ammonium nitrate with temperature. *J. Am. Chem. Soc.* **1932**, *54*, 2766–2786. [[CrossRef](#)]
26. Biessikirski, A.; Kuterasiński, Ł. Morphological properties of ANFO explosives obtained with the use of liquid combustibles. *Przem. Chem.* **2018**, *97*, 587–590.
27. Vargeese, A.A.; Joshi, S.S.; Krishnamurthy, V.N. Effect of method of crystallization on the IV-III and IV-II polymorphic transitions of ammonium nitrate. *J. Hazard. Mater.* **2009**, *161*, 373–379. [[CrossRef](#)] [[PubMed](#)]
28. Huelser, T.; Schnurre, S.M.; Wiggers, H.; Schulz, C. *Gas-Phase Synthesis of Highly-Specific Nanoparticles on the Pilot-Plant Scale*; NSTI-Nanotech: Anaheim, CA, USA, 2010.

29. Buczkowski, B.; Zygmunt, B. Modification of ammonium nitrate granules physical structure for ANFO production. *Przem. Chem.* **2008**, *87*, 707–710.
30. Lotspeich, E.; Petr, V. The characterization of ammonium nitrate mini-prills. In *Dynamic Behavior of Materials, Proceedings of the 2014 Annual Conference on Experimental and Applied Mechanics, Lombard, IL, USA, 3–5 June 2014*; Song, B., Casem, D., Kimberley, J., Eds.; Springer: Cham, Switzerland, 2015; Volume 1, pp. 319–325.
31. Biessikirski, A.; Kuterasiński, Ł. *Research on Morphology and Topology of ANFO Based on Various Types of Oxygen Component*; Wydawnictwa AGH: Kraków, Poland, 2018.
32. Rao, K.V.R.; Hariharan, P.L.; Jagannathan, K.; Yoganarasimhan, S.R. Scanning electron microscopy of ammonium nitrate prills in relations to their application in ammonium nitrate–fuel oil systems. *Fuel* **1989**, *68*, 1118–1122.
33. Viktorov, S.D.; Frantov, A.E.; Lapikov, I.N.; Andreev, V.V.; Starshinov, A.V. Effect of the microstructure of ammonium nitrate granules on the detonability of composite propellants based on it. *Combust. Explos. Shock. Waves* **2016**, *52*, 727–731. [[CrossRef](#)]
34. Biessikirski, A. *Research on the Physicochemical Properties of Non-ideal Explosives Based on Various Types of Ammonium Nitrate(V) and Fuel Oils*; Wydawnictwa AGH: Kraków, Poland, 2020.